

Non-Hermitian Photonics based on Charge-Parity Symmetry

Junpeng Hou,¹ Zhitong Li,² Qing Gu,² and Chuanwei Zhang¹

¹*Department of Physics, The University of Texas at Dallas, Richardson, Texas 75080-3021, USA*

²*Department of Electrical and Computer Engineering,
The University of Texas at Dallas, Richardson, Texas 75080-3021, USA*

Parity-time (\mathcal{PT}) symmetry, originally conceived for non-Hermitian open quantum systems, has opened an excitingly new avenue for the coherent control of light. By tailoring optical gain and loss in integrated photonic structures, \mathcal{PT} symmetric non-Hermitian photonics has found applications in many fields ranging from single mode lasing to novel topological matters. Here we propose a new paradigm towards non-Hermitian photonics based on the charge-parity (\mathcal{CP}) symmetry that has the potential to control the flow of light in an unprecedented way. In particular, we consider continuous dielectric chiral materials, where the charge conjugation and parity symmetries are broken individually, but preserved jointly. Surprisingly, the phase transition between real and imaginary spectra across the exceptional point is accompanied by a dramatic change of the photonic band topology from dielectric to hyperbolic. We showcase broad applications of \mathcal{CP} symmetric photonics such as all-angle polarization-dependent negative refraction materials, enhanced spontaneous emission for laser engineering, and non-Hermitian topological photonics. The \mathcal{CP} symmetry opens an unexplored pathway for studying non-Hermitian photonics without optical gain/loss by connecting two previously distinct material properties: chirality and hyperbolicity, therefore providing a powerful tool for engineering many promising applications in photonics and other related fields.

Originally conceived for open quantum systems [1], \mathcal{PT} symmetry was later introduced to photonics through the analogy between Schrödinger equation and Maxwell equations under paraxial approximation [2, 3]. \mathcal{PT} symmetry allows real eigenspectrum for a class of non-Hermitian Hamiltonians [3, 4], which support two distinct phases: \mathcal{PT} -symmetric (real eigenfrequencies) and \mathcal{PT} -broken (both real and complex eigenfrequencies), as illustrated in Fig. 1(a). The phase transition between them is characterized by the exceptional point [5]. In photonics, non-Hermitian Hamiltonian with \mathcal{PT} symmetry can be engineered through tuning optical gain and loss of materials, which provides a powerful tool for shaping the flow of light and yields novel applications in nonlinear optics [6], lasing [7, 8], unidirectional propagation [9], precise sensing [10], topological photonics [11, 12], etc.

The significance of \mathcal{PT} symmetric photonics naturally raises the question whether there is non-Hermitian photonics protected by other types of symmetries. Note that the \mathcal{PT} symmetry for photonics is based on the paraxial approximation of Maxwell equations, which describe the multiple-component electromagnetic field and could be non-Hermitian even without optical gain/loss. In this Letter, we propose a new class of non-Hermitian photonics based on the \mathcal{CP} symmetry of Maxwell equations, where \mathcal{C} represents charge-conjugation. Similar to \mathcal{PT} symmetry, there are two distinct phases: \mathcal{CP} -symmetric with real eigenfrequencies and \mathcal{CP} -broken with complex eigenfrequencies. Such \mathcal{CP} symmetric non-Hermitian photonics can exist, for instance, in a continuous dielectric media with proper chiral effects. An example is provided in Fig. 1(b), where the spectrums are two-fold degenerate. The transition between \mathcal{CP} -symmetric and -broken phases can occur at points, lines, or surfaces

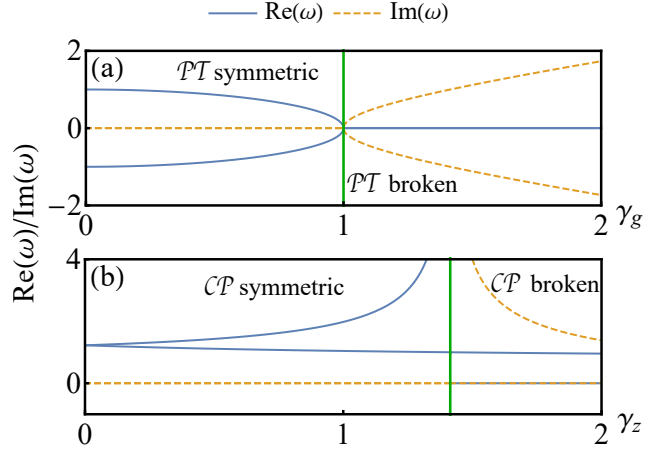


FIG. 1: **Eigenfrequency spectrums for non-Hermitian photonics with (a) \mathcal{PT} and (b) \mathcal{CP} symmetries.** Solid blue and dashed orange curves represent real and imaginary parts of the eigenfrequencies. For the \mathcal{CP} case, each curve is two-fold degenerate with different eigenstates. The green vertical lines indicate the exceptional points, at which the Hamiltonian is defective. The driving terms for the symmetry breaking are gain/loss γ_g and chiral effect γ_z , respectively. At the exceptional point, a pair of eigenmodes become degenerate at $\omega = 0$ for \mathcal{PT} symmetry breaking, while diverge for \mathcal{CP} symmetry breaking. The spectrums for the latter case are computed at $\mathbf{k} = 1$ in a chiral dielectric $\epsilon = 2$ and $\mu = 1$.

in either parameter or momentum space. The transition points are analogous to the exceptional points in \mathcal{PT} -symmetry in the sense of defective Hamiltonians, therefore we still name them as exceptional points. However, at the exceptional points, the eigenfrequencies (both real and imaginary parts) diverge (Fig. 1(b)) for the \mathcal{CP} -symmetry, in contrast to the degeneracy at finite values

for the \mathcal{PT} -symmetry (Fig. 1(a)).

The transition between \mathcal{CP} -symmetric and -broken phases is accompanied by a surprising change of the photonic band topology. In the \mathcal{CP} -symmetric phase, the band is still dielectric with elliptical equal frequency surface (EFS), while in the \mathcal{CP} -broken phase, the band dispersion becomes hyperbolic with indefinite bands. The hyperbolic band dispersion is a unique feature of hyperbolic metamaterials (HMMs) [13, 14], which are usually implemented by creating a metal-dielectric composite to achieve metal and dielectric properties in orthogonal directions. HMMs have found great applications in versatile fields like negative refraction [15, 16], enhanced spontaneous emission [17–21], super-resolution imaging [22, 23], bio-sensing [24], and topological photonics [25–27]. The chirality driven hyperbolic bands through \mathcal{CP} -symmetry breaking provides a new route for realizing hyperbolic materials in all-dielectric media for the first time, leading to lossless hyperbolic dielectric materials. The \mathcal{CP} -symmetric physics enables broadly and promisingly technologic applications, and here we showcase a few examples including all-angle polarization-dependent negative refraction, enhanced spontaneous emission, and non-Hermitian topological phases.

Symmetries of Maxwell equations. We consider a continuous photonic medium that can be described by Maxwell equations in the extended eigenvalue-problem form $H_P\psi = \omega H_M\psi$ with

$$H_P = i \begin{pmatrix} 0 & \nabla \times \\ -\nabla \times & 0 \end{pmatrix}, H_M = \begin{pmatrix} \epsilon & i\gamma \\ -i\gamma & \mu \end{pmatrix}, \psi = \begin{pmatrix} \mathbf{E} \\ \mathbf{H} \end{pmatrix}. \quad (1)$$

Here the chiral term $\gamma = \text{Tr}(\gamma)I_3/3 + N$ [28] couples \mathbf{E} (\mathbf{D}) and \mathbf{B} (\mathbf{H}), I_3 is the 3×3 identity matrix, and N is a symmetric traceless matrix. For a homogeneous medium, $H(-\mathbf{k}) = -H(\mathbf{k})$ with $H(\mathbf{k}) = H_M^{-1}H_P(\mathbf{k})$ [27], dictating that eigenmodes $\omega_{\mathbf{k}}$ and $-\omega_{-\mathbf{k}}$ represent the same physical state.

The time-reversal symmetry operator is defined as $\mathcal{T} = \sigma_z \otimes I_3 K$, where the Pauli matrix σ_i is defined on the (\mathbf{E}, \mathbf{H}) basis [29]. Preserving \mathcal{T} symmetry requires $\epsilon^* = \epsilon$, $\mu^* = \mu$, therefore gyromagnetic effect or material gain/loss breaks time-reversal symmetry. The parity symmetry operator $\mathcal{P} = -\sigma_z \otimes I_3$ satisfies $\mathcal{P}H_P(\mathbf{k})\mathcal{P}^{-1} = H_P(-\mathbf{k})$, $\det(\mathcal{P}) = -1$ [31], and $\mathcal{P} \begin{pmatrix} \mathbf{E} \\ \mathbf{H} \end{pmatrix} = \begin{pmatrix} -\mathbf{E} \\ \mathbf{H} \end{pmatrix}$ as expected. The Hamiltonian $H(\mathbf{k})$ has an even parity $\mathcal{P}H(-\mathbf{k})\mathcal{P}^{-1} = H(\mathbf{k})$ when $\gamma = 0$, and the parity operator changes the sign of the chirality γ [28]. Because photons are gauge bosons without mass and charge, the charge-conjugation is defined as $\mathcal{C} = -K$ such that $\mathcal{CPT} = 1$ [32].

In an ideal dielectric (HMM or metal) that only have real permittivity and permeability vectors, these three symmetries are persevered individually. While each of them can be broken explicitly, $\mathcal{CPT} = 1$ is always pre-

Symmetry	Eigenmodes	Breaking mechanism(s)
\mathcal{T}	$\omega_{\mathbf{k}} \rightarrow \omega_{-\mathbf{k}}^*$	Gain/loss, gyromagnetic
\mathcal{C}	$\omega_{\mathbf{k}} \rightarrow \omega_{\mathbf{k}}^*$	Gain/loss, chiral, gyromagnetic
\mathcal{CT}	$\omega_{\mathbf{k}} \rightarrow \omega_{\mathbf{k}}^*$	Gain/loss, gyromagnetic
\mathcal{P}	$\omega_{\mathbf{k}} \rightarrow \omega_{-\mathbf{k}}$	Chiral
\mathcal{PT}	$\omega_{\mathbf{k}} \rightarrow \omega_{-\mathbf{k}}$	Cannot be broken

TABLE I: **Symmetries of Maxwell equations.** Some important symmetries, together with their actions on eigenmodes and breaking methods, are listed for $H(\mathbf{k})$. Besides \mathcal{CPT} , two symmetries $H(-\mathbf{k}) = -H(\mathbf{k})$ and \mathcal{PT} are always preserved.

served. Note that the chiral term $\gamma = \omega g$ [33], thus the signs of eigenfrequency and chiral term are not independent. A chiral inversion operator $\Gamma : \gamma \rightarrow -\gamma$ can be defined, which yields an additional symmetry $(\mathcal{PT})H(\mathbf{k})(\mathcal{PT})^{-1} = -H(\mathbf{k})$, dictating that there are only two independent non-zero modes. Hereafter we choose both modes with $\Re(\omega) > 0$ (< 0) for a given chiral term γ ($-\gamma$) [27]. The above symmetries of Maxwell equations and their consequences are summarized in Tab. I.

Interesting physics arises when a combination of two symmetries, such as \mathcal{PT} or \mathcal{CP} , is preserved while each is individually broken. Here we consider non-Hermitian photonics based on \mathcal{CP} symmetry. Consider the two eigenmodes $\psi_{j,\mathbf{k}}$ with eigenfrequencies $\omega_{j,\mathbf{k}}, j = 0, 1$ of the Maxwell equations. Under \mathcal{CP} symmetry, $(\mathcal{CP})H(\mathbf{k})(\mathcal{CP})^{-1} = H(-\mathbf{k})$, meaning $\omega_{j,-\mathbf{k}}$ is also an eigenfrequency. Notice that the constantly preserved $(\mathcal{PT})H(\mathbf{k})(\mathcal{PT})^{-1} = H(-\mathbf{k})$ symmetry, yields that $\omega_{j,\mathbf{k}} = \omega_{j,-\mathbf{k}}$. Note that, such a constraint always applies and it gives rise to the two-fold degeneracy in Fig. 1(b).

Therefore, in the \mathcal{CP} symmetric regime, the combination of the above two conditions gives $\omega_{j,\mathbf{k}} = \omega_{j,-\mathbf{k}}^* = \omega_{j,\mathbf{k}}^*$. This imposes the reality of eigenfrequency spectrum. In this symmetric regime, the eigenstates also obey the transformation relation given by the \mathcal{CP} symmetry, i.e., $(\mathcal{CP})\psi_{j,\mathbf{k}} = e^{i\theta_j}\psi_{j,-\mathbf{k}}$. There also exists the \mathcal{CP} -broken regimes, where \mathcal{CP} symmetry relates the two states for a given j at the same, instead of opposite, momenta. This leads to the constraints on eigenstates $(\mathcal{CP})\psi_{j,\pm\mathbf{k}} = e^{i\theta_{j,\pm\mathbf{k}}}\psi_{j,\pm\mathbf{k}}$, meaning the eigenfrequencies must be purely imaginary since $\omega_{j,\pm\mathbf{k}} = -\omega_{j,\pm\mathbf{k}}^*$.

\mathcal{CP} symmetric photonics in a chiral medium. The chiral term γ breaks \mathcal{C} and \mathcal{P} symmetries individually, but preserves the combined \mathcal{CP} symmetry, therefore chiral media provide an excellent platform for exploring non-Hermitian photonics based on \mathcal{CP} symmetry. Chirality is ubiquitous in many different materials, and in photonics chirality gives rise to unique wave propagations [33]. However, chiral effects are usually weak in natural materials. Recently, rapid development of chiral metamaterials [34–36] and chiral plasmonics [37] has opened the

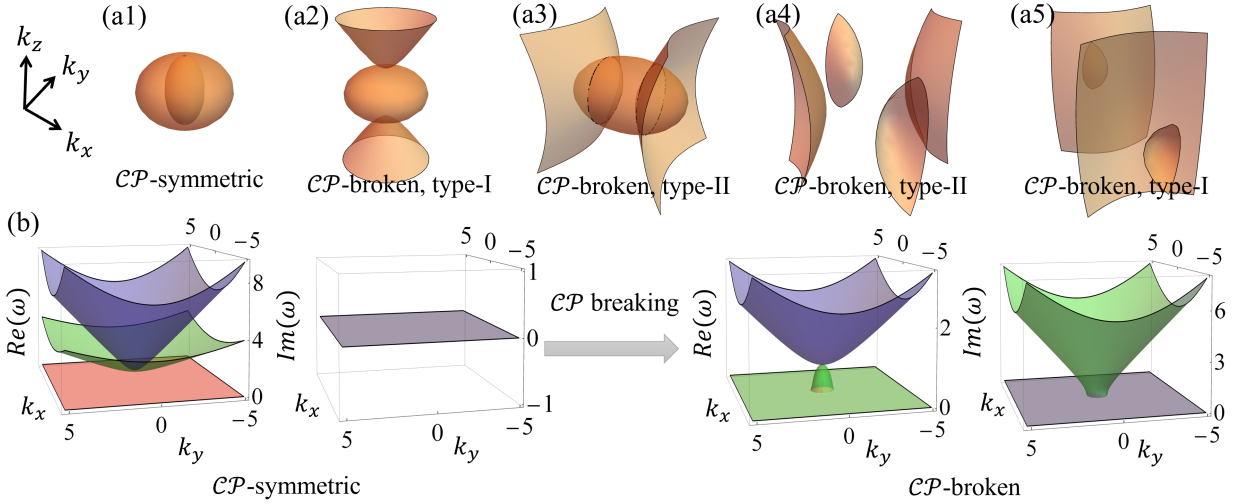


FIG. 2: **\mathcal{CP} breaking and hyperbolicity.** (a) Some examples of EFSs at $\omega = 1$ in \mathcal{CP} -symmetric (-broken) regions. We define the type-I and type-II HMMs according to $\det(H_M) < 0$ and $\det(H_M) > 0$ respectively. From left to right, we choose $\gamma = \text{diag}(0, 0, 1)$, $\gamma = \text{diag}(0, 0, 2)$, $\gamma = \text{diag}(0, 2, 2)$, $(\gamma_x, \gamma_y, \gamma_{xy}, \gamma_{yx}) = (1, 1, 3, 3)$ and $(\gamma_x, \gamma_y, \gamma_z, \gamma_{xy}, \gamma_{yx}) = (1, 1, 2, 3, 3)$. (b) Dielectric real bands (a1) change to type-I hyperbolic complex bands (a2) across \mathcal{CP} symmetry breaking in momentum space $k_z = 1$. For all panels, $\epsilon_D = 2$ and $\mu_D = 1$.

door for realizing strong chiral media in a wide range of frequencies including microwave, terahertz, infrared and visible frequencies. Besides enhanced circular dichroism and optical activity [34–37], strong chiral media also exhibits negative refraction for certain incident angles [38–41].

For better illustration of \mathcal{CP} symmetry effects, we consider an isotropic dielectric $\epsilon = \epsilon_D I_3, \epsilon_D \geq 0$, $\mu = \mu_D I_3, \mu_D > 0$ with only real diagonal chiral term $\gamma = \text{diag}(\gamma_x, \gamma_y, \gamma_z)$. Such chiral term breaks \mathcal{C} , \mathcal{P} respectively, but preserves their combination \mathcal{CP} (see Tab. I). A simple but instructive case is $\gamma = \text{diag}(0, 0, \gamma_z > 0)$. The EFS can be determined by

$$\epsilon_D \mu_D (k_t^2 + k_z^2 - \epsilon_D \mu_D \omega^2)^2 = \gamma_z^2 (k_z^2 - \epsilon_D \mu_D \omega^2)^2, \quad (2)$$

which has four solutions in general

$$k_z = \pm \sqrt{f_{\pm}(\gamma_z) k_t^2 + \omega^2 \epsilon_D \mu_D}, \quad (3)$$

where $f_{\pm}(\gamma_z) = \frac{\sqrt{\epsilon_D \mu_D}}{\pm \gamma_z - \sqrt{\epsilon_D \mu_D}}$ and $k_t^2 = k_x^2 + k_y^2$.

For a small $\gamma_z < \sqrt{\epsilon_D \mu_D}$, $f_{\pm}(\gamma_z)$ are both negative, therefore the EFS is bounded and elliptical, which is essentially the same as a dielectric (see Fig. 2(a1)), except that the degeneracy between different polarizations is lifted. All eigenfrequencies are real and the same at $\pm \mathbf{k}$. The eigenmodes with nonzero eigenfrequencies satisfy $(\mathbf{E}_{\mathbf{k}}, \mathbf{H}_{\mathbf{k}})_j = e^{i\theta_j} (-\mathbf{E}_{-\mathbf{k}}, \mathbf{H}_{-\mathbf{k}})_j$, demonstrating the \mathcal{CP} -symmetric phase.

At the exceptional point $\gamma_z^c = \sqrt{\epsilon_D \mu_D}$, $f_+(\gamma_z)$ diverges and the Hamiltonian $H(\mathbf{k})$ is ill-defined because $\det(H_M) = 0$. There are only two solutions for $f_-(\gamma_z)$ with $k_z = \pm \sqrt{-k_t^2/2 + \omega^2 \epsilon_D \mu_D}$. The non-Hermitian

Hamiltonian $H(\mathbf{k})$ is defective at the exceptional point in the sense that the number of linearly independent eigenmodes is less than the dimension of the Hamiltonian, which is different from the defectiveness of \mathcal{PT} -symmetric Hamiltonians at the exceptional point that have coalesced eigenstates (i.e., linearly dependent).

Beyond the exceptional point $\gamma_z > \gamma_z^c$, two purely imaginary eigenmodes appear, which denotes the \mathcal{CP} -broken regime. Meanwhile, $f_+(\gamma_z)$ becomes positive, leading to the indefinite (hyperbolic) bands, as shown in Fig. 2(a2), which are similar to type-I HMMs. In Fig. 2(b), we plot the complex band structures at a finite k_z across the \mathcal{CP} breaking transition. Before the transition $\gamma_z < \gamma_z^c$, the degenerate bands (blue and green) at $\gamma_z = 0$ split but remain real in the entire momentum space. The red plane represents static solutions of Maxwell equations, which are zero for any chiral term. With increasing γ_z , the lower band is gradually flattened. Across the exceptional point γ_z^c , the real part of the lower band manifests as a cone located at the origin with a quadratic band touching with the upper band, while the rest parts become purely imaginary. Such band dispersion exhibits an exceptional ring on the k_x - k_y plane (an exceptional cone in 3D momentum space), where the eigenmodes coalesce to zero eigenfrequency and null eigenvector.

The existence of multiple chiral terms along different directions provide a tunable tool for driving \mathcal{CP} breaking transition and engineering different hyperbolic band dispersions. In the case $\gamma = \text{diag}(\gamma_x, \gamma_y, \gamma_z)$, there exists three individual exceptional points at $\gamma_l^c = \sqrt{\epsilon_D \mu_D}, l = x, y, z$ along each spatial direction. When all $\gamma_l < \sqrt{\epsilon_D \mu_D}$, the system remains \mathcal{CP} symmetric and

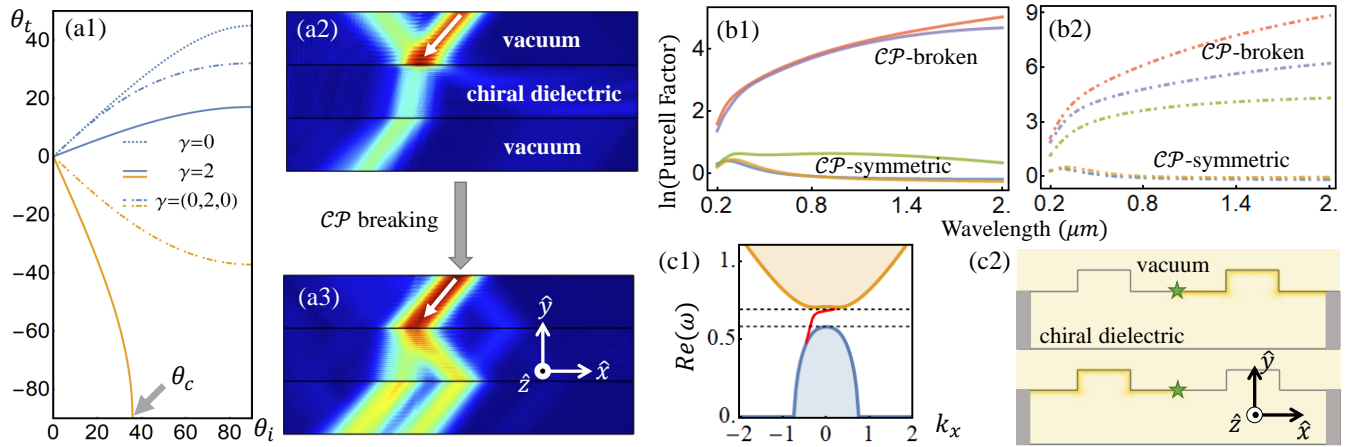


FIG. 3: **Applications of \mathcal{CP} -symmetric photonics.** (a) All-angle and polarization-dependent negative refraction. (a1) Analytic calculations of a linearly polarized plane wave transmitting on the boundary between a chiral dielectric and vacuum. The plot shows transmitted angle θ_t with respect to different incident angle θ_i . The blue and khaki curves represent right-handed and left-handed polarizations. (a2-a3) COMSOL simulations for (a1). Incident angle is fixed at $\theta_i = 40^\circ$ while $\gamma = 2I_3$ and $\gamma = \text{diag}(0, 2, 0)$ for the upper and lower panel. The white arrows denote the incident directions. (b) Isotropic Purcell factor for \mathcal{CP} symmetric dielectric with (b1) type-I and (b2) type-II hyperbolic dispersions after symmetry breaking. A leap of Purcell factor is observed across the exceptional point. (c) Topological physics in the \mathcal{CP} -broken phase. (c1) 2D band structure at $k_z = 1$ with open boundary condition along y . Two dashed lines give the band gap 0.58 to 0.69 and the red curve represents chiral surface wave. (c2) COMSOL simulations for $k_z = 1$ (upper) and $k_z = -1$ (lower). The green star denotes the location of a line source and the corresponding input energy is $\omega = 0.59$. The grey areas represent absorption materials. For all panels, $\epsilon_D = 2$ and $\mu_D = 1$.

have ellipsoid EFSs. When one chiral term such as γ_z exceeds γ_z^c , the system enters the \mathcal{CP} -broken phase and exhibits hyperbolic dispersion, as shown in Figs. 2(a2) and (b). When γ_y also exceeds the exceptional point, the hyperbolic dispersion changes from type-I to type-II (see Fig. 2(a3)), and the cone-like EFSs lie along the k_x direction, which is perpendicular to the k_z - k_y plane. Interestingly, when all three chiral components exceeds γ_l^c , the system transitions back to the \mathcal{CP} -symmetric phase and the hyperbolic dispersions disappear. This feature is unique to \mathcal{CP} symmetric systems, because in \mathcal{PT} symmetric systems, one always ends up in the \mathcal{PT} -broken regime with increasing material gain/loss strength. More exotic hyperbolic band dispersions, which cannot be realized in metal-dielectric patterned HMMs, can be engineered through \mathcal{CP} -breaking when non-diagonal chiral terms are involved, as shown in two examples illustrated in Figs. 2(a4) and (a5). More details on the \mathcal{CP} -breaking-induced hyperbolicity are presented in Supplemental Note [30]. These results clearly showcase that strong chiral materials may provide a tunable platform for realizing lossless hyperbolic materials and significantly broadening the applications of HMMs.

Applications of \mathcal{CP} breaking. Due to the rise of hyperbolicity, the non-Hermitian photonics based upon \mathcal{CP} symmetry may have potential applications in a plethora of fields. In the following, we briefly illustrate three applications covering classical optics, laser engineering, and topological photonics, and leave the technical details in

Supplemental Notes [30].

All-angle polarization-dependent beam splitter: Birefringence and negative refraction have long been studied in chiral media and it is known that there is a critical angle θ_c , beyond which one polarization is totally reflected. The critical angle vanishes in \mathcal{CP} -broken regimes because the negative refraction has been promoted to an all-angle effect thanks to indefinite bands, as demonstrated by the analytic results (Fig. 3(a1)), together with the COMSOL simulation (Figs. 3(a2,a3)). Because of the polarization dependence of the chiral media shown in Fig. 3(a), the \mathcal{CP} -symmetric photonics promises an all-angle polarization-dependent beam splitter, a device that is hard to engineer in either isotropic chiral materials or HMM.

Enhanced spontaneous emissions for laser engineering: Spontaneous emissions play a crucial role for laser engineering, and have been widely studied in chiral media, but mainly in the \mathcal{CP} -symmetric regime. The hyperbolic bands in the \mathcal{CP} -broken regime can significantly enhance the spontaneous emissions of a dielectric continuum with both broader bandwidth and stronger Purcell effect. For simplicity, we assume a frequency-independent permeability constant and compute the isotropic Purcell factor in Fig. 3(b). Upon crossing the exceptional point, a large leap of the Purcell factor is observed.

Topological photonics: Interestingly, the \mathcal{CP} breaking transition could also be a topological one, leading to

a non-trivial topological phase in the \mathcal{CP} -broken phase. The topological properties of a \mathcal{CP} -broken chiral dielectric is similar to that of a Weyl semimetal but the Weyl point is replaced by a charge-2 triply-degenerate point [27, 42] at $\mathbf{k} = 0$ (see Supplemental Note [30] for more details). At a finite k_z , the quadratic band touching in Fig. 2(b) may be lifted by anisotropy of ϵ and the projected 2D band structure with chiral surface wave is plotted in Fig. 3(c1). Such chiral edge states are confirmed in COMSOL simulation (Fig. 3(c2)), where we see the chirality of edge states is associated with the sign of k_z due to the breaking of \mathcal{P} . Note that the edge modes respect \mathcal{CP} symmetry even though it is broken in the bulk, therefore the edge modes have only real eigenfrequencies.

Conclusion and Discussion. In conclusion, we propose a new class of non-Hermitian photonics based on \mathcal{CP} symmetry, which shares certain similarity, but is dramatically different from the well-known \mathcal{PT} -symmetric photonics. The physical realization of such \mathcal{CP} -symmetric photonics in chiral dielectrics opens a novel pathway for engineering exotic hyperbolic materials with significant applications. Our work may shed light on future experimental and theoretical development of new non-Hermitian photonics.

Many important questions remain to be answered for the \mathcal{CP} -symmetric non-Hermitian photonics and here we list a few of them: *i*) Can \mathcal{CP} symmetry and its breaking be induced by means other than chiral effects? *ii*) Can \mathcal{CP} symmetric photonics be applied to periodic optical systems like photonic crystals or coupled optical cavities? *iii*) Are there other paths to non-Hermitian photonics besides \mathcal{PT} and \mathcal{CP} symmetries? *iv*) Finally, does such \mathcal{CP} -symmetric non-Hermitian physics exist in physical systems other than photonics?

Acknowledgements: This work was supported by Air Force Office of Scientific Research (FA9550-16-1-0387), National Science Foundation (PHY-1505496, PHY-1806227), and Army Research Office (W911NF-17-1-0128). Z. Li and Q. Gu acknowledge funding from UT Dallas faculty start-up funding.

-
- [1] C. M. Bender and S. Boettcher, Real Spectra in Non-Hermitian Hamiltonians Having PT Symmetry, *Phys. Rev. Lett.* **80**, 5243 (1998).
- [2] M. Lax, W. H. Louisell, and W. B. McKnight, From Maxwell to paraxial wave optics, *Phys. Rev. A* **11**, 1365 (1975).
- [3] L. Feng, R. El-Ganainy & L. Ge, Non-Hermitian photonics based on parity-time symmetry, *Nat. Photonics* **11**, 752 (2017).
- [4] R. El-Ganainy, K. G. Makris, M. Khajavikhan, Z. H. Musslimani, S. Rotter & D. N. Christodoulides, Non-Hermitian physics and PT symmetry, *Nat. Phys.* **14**, 11 (2018).
- [5] W. D. Heiss, Exceptional points of non-Hermitian operators, *J. Phys. A: Math. Gen.* **37**, 2455 (2004).
- [6] M. Wimmer, A. Regensburger, M.-A. Miri, C. Bersch, D. N. Christodoulides & U. Peschel, Observation of optical solitons in PT-symmetric lattices, *Nat. Commun.* **6**, 7782 (2015).
- [7] H. Hodaei, M.-A. Miri, M. Heinrich, D. N. Christodoulides, M. Khajavikhan, Parity-time-symmetric microring lasers, *Science* **346**, 975 (2018).
- [8] J. Zhang et al, A phonon laser operating at an exceptional point, *Nat. Photonics* **12**, 479 (2018).
- [9] Z. Lin, H. Ramezani, T. Eichelkraut, T. Kottos, H. Cao, and D. N. Christodoulides, Unidirectional Invisibility Induced by PT-Symmetric Periodic Structures, *Phys. Rev. Lett.* **106**, 213901 (2011).
- [10] W. Chen, J. Zhang, B. Peng, S. K. Özdemir, X. Fan, and L. Yang, Parity-time-symmetric whispering-gallery mode nanoparticle sensor, *Photonics Research* **6**, A23 (2018).
- [11] S. Weimann et al., Topologically protected bound states in photonic parity-time-symmetric crystals, *Nat. Mater.* **16**, 433 (2017).
- [12] M. Pan, H. Zhao, P. Miao, S. Longhi & L. Feng, Topologically protected bound states in photonic parity-time-symmetric crystals, *Nat. Commun.* **9**, 1308 (2018).
- [13] D. R. Smith and D. Schurig, Electromagnetic Wave Propagation in Media with Indefinite Permittivity and Permeability Tensors, *Phys. Rev. Lett.* **90**, 077405 (2003).
- [14] A. Poddubny, I. Iorsh, P. Belov, and Y. Kivshar, Hyperbolic metamaterials, *Nat. Photonics* **7**, 958 (2013).
- [15] Y. Liu, G. Bartal, and X. Zhang, All-angle negative refraction and imaging in a bulk medium made of metallic nanowires in the visible region, *Opt. Express* **16**, 15439 (2008).
- [16] M. Shoaie, M. Kazem Moravvej-Farshi, and L. Yousefi, All-optical switching of nonlinear hyperbolic metamaterials in visible and near-infrared regions, *J. Opt. Soc. Am. B* **32**, 2358 (2015).
- [17] L. Ferrari, D. Lu, D. Lepage, and Z. Liu, Enhanced spontaneous emission inside hyperbolic metamaterials, *Opt. Express* **22**, 4301 (2014).
- [18] D. Lu, J. J. Kan, E. E. Fullerton, and Z. Liu, Enhancing spontaneous emission rates of molecules using nanopatterned multilayer hyperbolic metamaterials, *Nat. Nanotechnol.* **9**, 48 (2014).
- [19] L. Ferrari, J. S. T. Smalley, Y. Fainman, and Z. Liu, Hyperbolic metamaterials for dispersion-assisted directional light emission, *Nanoscale* **9**, 9034 (2014).
- [20] T. Galfsky, Z. Sun, C. R. Consideine, C. T. Chou, W. C. Ko, Y. H. Lee, E. E. Narimanov, and V. M. Menon, Broadband Enhancement of Spontaneous Emission in Two-Dimensional Semiconductors Using Photonic Hypercrystals, *Nano Lett.* **16**, 4940 (2016).
- [21] R. Chandrasekar et al, Lasing Action with Gold Nanorod Hyperbolic Metamaterials, *ACS Photonics* **4**, 674 (2017).
- [22] Z. Jacob, L. V. Alekseyev, and E. Narimanov, Optical Hyperlens: Far-field imaging beyond the diffraction limit, *Opt. Express* **14**, 8247 (2006).
- [23] Z. Liu, H. Lee, Y. Xiong, C. Sun, and X. Zhang, Far-field optical hyperlens magnifying sub-diffraction-limited objects, *Science* **315**, 1686 (2007).
- [24] A. V. Kabashin et al, Plasmonic nanorod metamaterials for biosensing, *Nat. Mater.* **8**, 867 (2009).
- [25] W. Gao et al, Topological Photonic Phase in Chiral Hyperbolic Metamaterials, *Phys. Rev. Lett.* **114**, 037402 (2015).
- [26] R.-L. Chern and Y. Z. Yu, Chiral surface waves on

- hyperbolic-gyromagnetic metamaterials, *Opt. Express* **25**, 11801 (2017).
- [27] J. Hou, Z. Li, X.-W. Luo, Q. Gu, C. Zhang, Topological bands and triply-degenerate points in non-Hermitian hyperbolic metamaterials, [arXiv 1808.06792](https://arxiv.org/abs/1808.06792) (2018).
- [28] A. J. Viitanen, A. Sihvola, I. V Lindell, and S. Tretyakov, *Electromagnetic Waves in Chiral and Bi-isotropic Media*, Artech Print (1994).
- [29] L. Lu, J. D. Joannopoulos & M. Soljacic, Topological photonics, *Nat. Photonics* **8**, 821 (2014).
- [30] See Supplemental Notes for more information.
- [31] A. Zee, *Group Theory in a Nutshell for Physicists*, Princeton University Press (2016).
- [32] The \mathcal{CPT} symmetris here are all classical and should not be confued with those in quantum field theory, in which \mathcal{C} is always respected by electromagnetism. See references, e.g., M. E. Peskin, D. V. Schroeder, *An Introduction to Quantum Field Theory*, Addison Wesley (1997).
- [33] J. Lekner, Optical properties of isotropic chiral media, *J. Opt.* **5**, 417 (1996).
- [34] S. S. Oh and O. H. author, Chiral metamaterials: enhancement and control of optical activity and circular dichroism, *Nano Convergence* **2**, 24 (2015).
- [35] Z. Wang, F. Cheng, T. Winsor and Y. Liu, Optical chiral metamaterials: a review of the fundamentals, fabrication methods and applications, *Nanotechnology* **27**, 412001 (2016).
- [36] X. Ma, M. Pu, X. Li, Y. Guo, P. Gao and X. Luo, Meta-Chirality: Fundamentals, Construction and Applications, *Nanomaterials* **7**, 116 (2017).
- [37] M. Hentschel, M. Schäferling, X. Duan, H. Giessen and N. Liu, Chiral plasmonics, *Sci. Adv.* **3**, 5 (2017).
- [38] J. B. Pendry, A Chiral Route to Negative Refraction, *Science* **306**, 1353 (2004).
- [39] C. Monzon and D.W. Forester, Negative Refraction and Focusing of Circularly Polarized Waves in Optically Active Media, *Phys. Rev. Lett.* **95**, 123904 (2005).
- [40] R.-Lin. Chern, Wave propagation in chiral media: composite Fresnel equations, *J. Opt.* **15** 075702 (2013).
- [41] S. Zhang, Y.-S. Park, J. Li, X. Lu, W. Zhang, and X. Zhang, Negative Refractive Index in Chiral Metamaterials, *Phys. Rev. Lett.* **102**, 023901 (2009).
- [42] H. Hu, J. Hou, F. Zhang, and C. Zhang, Topological Triply Degenerate Points Induced by Spin-Tensor-Momentum Couplings, *Phys. Rev. Lett.* **120**, 240401 (2018).

\mathcal{C} , \mathcal{P} , and \mathcal{T} symmetries of Maxwell equations

The condition for persevering \mathcal{T} symmetry can be simply obtained from matching $\mathcal{T}H_M\mathcal{T}^{-1}$ with H_M since we already have $\mathcal{T}H_P\mathcal{T}^{-1} = H_P$. A simple calculation shows $\mathcal{T}H_M\mathcal{T}^{-1} = \begin{pmatrix} \epsilon^* & i\gamma \\ -i\gamma & \mu^* \end{pmatrix}$, which yields the condition shown in the main text.

One can easily verify that $\mathcal{P} = -\sigma_z \otimes I_3$ satisfies the following equations $\mathcal{P} \begin{pmatrix} 0 & \nabla \times \\ -\nabla \times & 0 \end{pmatrix} \mathcal{P}^{-1} = \begin{pmatrix} 0 & -\nabla \times \\ \nabla \times & 0 \end{pmatrix}$, $\mathcal{P} \begin{pmatrix} \mathbf{E} \\ \mathbf{H} \end{pmatrix} = \begin{pmatrix} -\mathbf{E} \\ \mathbf{H} \end{pmatrix}$, $\mathcal{P} \begin{pmatrix} \epsilon & i\gamma \\ -i\gamma & \mu \end{pmatrix} \mathcal{P}^{-1} = \begin{pmatrix} \epsilon & -i\gamma \\ i\gamma & \mu \end{pmatrix}$ and $|\mathcal{P}| = -1$. Therefore it fulfills all physical and mathematical requirements of a parity symmetry operator. Since H_P is even under \mathcal{P} and H_M is even when $\gamma = 0$, the system has even parity when $\gamma = 0$, regardless of the forms of μ and ϵ .

Photons are gauge bosons and their own antiparticles. Combining with the anti-linear requirement, we can reasonably guess the charge conjugation $\mathcal{C} = e^{i\theta_c} I_2 \otimes I_3 K$. Furthermore, $\mathcal{C}^2 = I_6$ because the system is expected to be invariant if the charge conjugation operation is applied twice. These observations lead to $\mathcal{C} = \pm K$, where we have dropped the identity matrix.

These choices are self-consistent in the sense that $\mathcal{C}\mathcal{P}\mathcal{T} = 1$ such that Maxwell equations remain invariant under $\mathcal{C}\mathcal{P}\mathcal{T}$. The matrix representations are valid only for Maxwell equations in the form of Equ. 1 and under the assumption of a spatially homogenous H_M .

An explicit example of $\mathcal{C}\mathcal{P}$ breaking

In the main text, we argue that the spontaneous breaking of $\mathcal{C}\mathcal{P}$ symmetry may lead to complex eigenmodes, which can be understood through the transformation of eigenmodes at $\pm \mathbf{k}$. If $(\mathcal{C}\mathcal{P})\psi_{j,\mathbf{k}} = e^{i\theta_j} \psi_{j,-\mathbf{k}}$, there is a constraint on eigenfrequencies $\omega_{j,\mathbf{k}} = \omega_{j,-\mathbf{k}}^*$, which dictates real spectrum. Here, we show an example in both $\mathcal{C}\mathcal{P}$ -symmetric and $\mathcal{C}\mathcal{P}$ -broken regions by writing down the eigenmodes explicitly. We take $\epsilon_D = 4$, $\mu_D = 1$, $\gamma = \text{diag}(0, 0, \gamma_z)$ and $\mathbf{k} = \mathbf{1}$. The exceptional point is then $\gamma_z^c = 2$.

There are two non-zero and positive (in $\mathcal{C}\mathcal{P}$ -symmetric regime) solutions $\omega_{0,\pm\mathbf{k}} = (6 - \gamma_z)/(2\gamma_{z,-})$ and $\omega_{1,\pm\mathbf{k}} = (6 + \gamma_z)/(2\gamma_{z,+})$ with eigenstates (but we can only take either the positive or negative branches for a given system)

$$\psi_{0,\pm\mathbf{k}} = ((i(2 - \gamma_z) \pm \gamma_{z,-})/8, (i(2 - \gamma_z) \mp \gamma_{z,-})/8, -i/2, (\gamma_z - 2 \pm i\gamma_{z,-})/4, (\gamma_z - 2 \mp i\gamma_{z,-})/4, 1)^T, \quad (4)$$

$$\psi_{1,\pm\mathbf{k}} = (-i(\gamma_z + 2) \pm \gamma_{z,+})/8, -i(\gamma_z + 2) \mp \gamma_{z,+})/8, i/2, -(\gamma_z + 2 \mp i\gamma_{z,+})/4, -(\gamma_z + 2 \pm i\gamma_{z,+})/4, 1)^T, \quad (5)$$

where $\gamma_{z,\pm} = \sqrt{(\gamma_z \pm 6)(\gamma_z \pm 2)}$.

When $0 < \gamma_z < \gamma_z^c$, $\gamma_{z,\pm} > 0$. It is obvious that $(\mathcal{C}\mathcal{P})\psi_{j,\mathbf{k}} = e^{i\pi} \psi_{j,-\mathbf{k}}$ such that $\omega_{j,\mathbf{k}} = \omega_{j,-\mathbf{k}}^*$, which is in the $\mathcal{C}\mathcal{P}$ -symmetric phase. When $\gamma_z > \gamma_z^c$, $\gamma_{z,+} > 0$ but $\gamma_{z,-}$ becomes purely imaginary. The condition $(\mathcal{C}\mathcal{P})\psi_{1,\mathbf{k}} = e^{i\pi} \psi_{1,-\mathbf{k}}$ survives, so we still see a real eigenmode. The transformation for the other one becomes $(\mathcal{C}\mathcal{P})\psi_{1,\pm\mathbf{k}} = e^{i\pi} \psi_{1,\pm\mathbf{k}}$, which requires $\omega_{1,\pm\mathbf{k}} = -\omega_{1,\pm\mathbf{k}}^*$. The $\mathcal{C}\mathcal{P}$ symmetry is partially broken by strong chiral effects and the eigenspectra become complex.

Hyperbolic bands from $\mathcal{C}\mathcal{P}$ breaking by chiral effects

The EFS for pure dielectric materials are spheres (ellipsoids) in the momentum space. However, the EFSs for HMMs are completely different as shown in Fig. 4(a,b), corresponding to type-I and type-II HMMs respectively [13, 14]. A significant feature of these EFSs is that they stretch to infinity in momentum space so that the material can support the propagation of large $|\mathbf{k}|$ waves. Such hyperbolicity was thought to be unique to HMMs [14]. Quite surprisingly, similar dispersions can also be realized through $\mathcal{C}\mathcal{P}$ -breaking induced by chiral terms. The corresponding EFSs are plotted in Fig. 4(c,d).

As observed in Fig. 4(c), chiral term along one spatial direction exceeding the exceptional point can render a dispersion relation mimicking that of a type-I HMM. If the chiral terms along two spatial directions exceed the exceptional points, the dispersion relation is similar as that for a type-II HMM, as shown in Fig. 4(d). Nevertheless, the geometries are not exactly the same in the small $|\mathbf{k}|$ region because we have two bounded EFSs surrounded by the hyperbolic one. While we have presented similar results and some exotic hyperbolic dispersions in the main text,

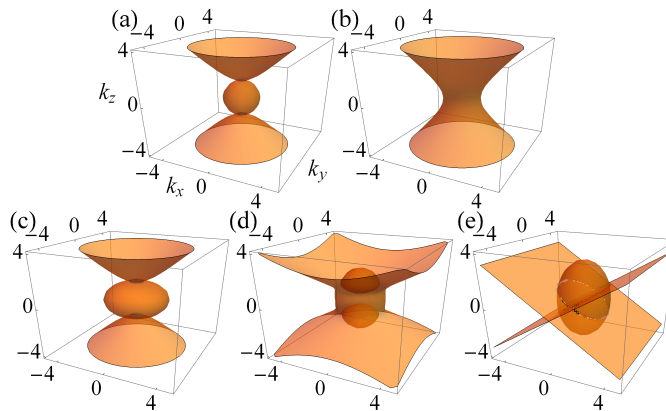


FIG. 4: Typical EFSs at $\omega = 1$ for type-I (a) and type-II (b) HMMs. We choose $\epsilon = \text{diag}(2, 2, -2)$ and $\epsilon = \text{diag}(-2, -2, 2)$ respectively. Corresponding realizations of dispersion relations in strong chiral dielectrics are shown in (c) $\epsilon = 2I_3$, $\gamma = \text{diag}(0, 0, 3)$, (d) $\epsilon = \text{diag}(1, 1, 2)$, $\gamma = \text{diag}(1.5, 1.5, 0)$ and (e) $\epsilon = \text{diag}(2, 2, 2)$ and $\gamma = \text{diag}(2, \sqrt{2}, 0)$. For all panels $\mu = I_3$.

Fig. 4(e) offers an example where the system is \mathcal{CP} -broken in one direction, and at the exceptional point in another direction.

In the following, we study the wave propagation in chiral media and show how the hyperbolic dispersions emerge. We first consider a chiral isotropic dielectric medium with constant scalar permittivity, permeability and chiral effect $\gamma = \gamma_D I_3$ as defined in the main text. This simple model is enough to gain insights into the systems and has been adopted frequently in previous literatures [33, 38–40]. The resulting dispersion relation

$$\omega = |\mathbf{k}| / |\sqrt{\epsilon_D \mu_D} \pm \gamma_D|. \quad (6)$$

For $\gamma_D = 0$, the EFS is a two-fold degenerate sphere as expected and the degeneracy comes from two different polarizations. For a finite chiral strength, the degeneracy is lifted and there are always two spheres with different radii in the momentum space except at $\gamma_D = \pm \sqrt{\epsilon_D \mu_D}$. It has been shown that for $|\gamma_D| > \sqrt{\epsilon_D \mu_D}$, there are negative refraction for proper incident angles because the time-averaged Poynting vector $\langle \mathbf{S} \rangle_t$ is antiparallel to \mathbf{k} [40]. This result is straightforward by noticing that the refraction indexes are $n = \sqrt{\epsilon_D \mu_D} \pm \gamma_D$ for right- and left-handed circular polarizations [35]. Nevertheless, the EFSs always remain ellipsoids for both $\gamma_D < \sqrt{\epsilon_D \mu_D}$ and $\gamma_D > \sqrt{\epsilon_D \mu_D}$ as a result of linear dispersion relations. Due to the bounded EFSs, there exists a critical angle θ_c in a scalar chiral medium, beyond which the incident waves with certain polarizations are totally reflected. A scalar chiral term cannot render spontaneous \mathcal{CP} breaking, which requires strong anisotropic chiral terms.

We now revisit the simple but instructive case in the main text with slightly different $\epsilon = \text{diag}(\epsilon_t > 0, \epsilon_t > 0, \epsilon_z > 0)$, $\mu = 1$ and $\gamma = \text{diag}(0, 0, \gamma_z)$. The dispersion relation becomes

$$(k_t^2 + k_z^2 - \epsilon_t \omega^2)(\epsilon_t k_t^2 + \epsilon_z k_z^2 - \epsilon_z \epsilon_t \omega^2) = \gamma_z^2 (k_z^2 - \epsilon_t \omega^2)^2, \quad (7)$$

where $k_t^2 = k_x^2 + k_y^2$. Our previous analysis suggests that there is an exceptional point $\gamma_z = \pm \sqrt{\epsilon_z}$ since γ_z is decoupled from k_x and k_y in Equ. 7. For a small γ_z , we have two distinguishable ellipsoids since the degeneracies between different polarizations are lifted. As the chiral strength increases, the inner EFS gets compressed along both k_x and k_y directions and disappears at the exceptional point. After passing the exceptional point, the EFSs are not two ellipsoids anymore because the leading term $(\epsilon_z - \gamma_z^2) \epsilon_t^2 \omega^4$ becomes negative, which mimics a type-I HMM. As a result, we observe type-I hyperbolic dispersions in the \mathcal{CP} -broken phase since hyperbolic bands must be non-Hermitian due to its metal character. Note that the two degenerate points at $\mathbf{k} = (0, 0, \pm k_z)$ survives, but can be lifted by anisotropy in permeability tensor $\epsilon_x \neq \epsilon_y$ or additional chiral terms.

Although the chirality induced hyperbolic dispersion shares a similar EFS to that for HMM, it is impossible to obtain a homogenous model for a strong chiral medium similar to that for a simple HMM. In a chiral medium, the eigenmodes with different polarizations are not degenerate. The existence of chiral effects also break all spatial inversion symmetries while a pure HMM preserves them. However, by comparing the wave equations in the frequency-momentum domain, we can recast the chiral medium with only non-zero γ_z into a “pure HMM” form

$$\epsilon_{eff} = (\epsilon_t, \epsilon_t, \epsilon_z - \gamma_z^2 (k_z^2 - \epsilon_t \omega^2) / (k_t^2 + k_z^2 - \epsilon_t \omega^2)), \quad (8)$$

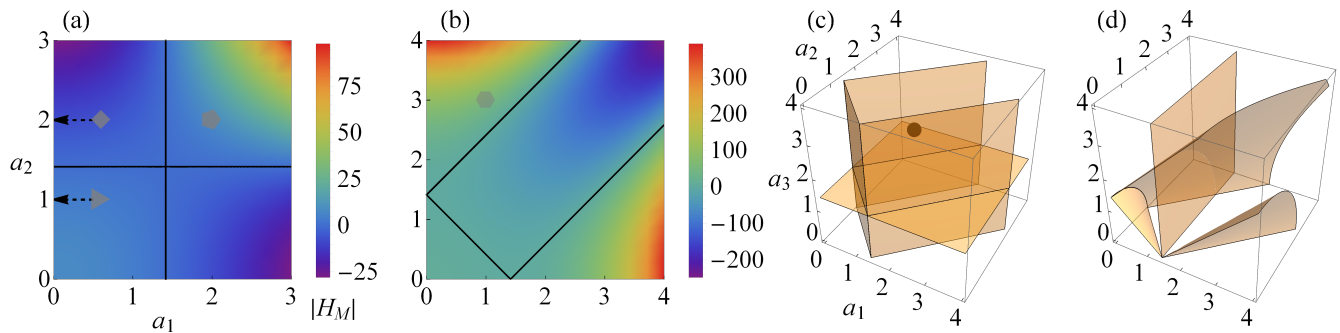


FIG. 5: Phase diagram plotted by $\det |H_M|$ for different chiral terms. (a) Density plot of $\det |H_M|$. The solid black curves denote zero solutions (exceptional points). $\gamma = \text{diag}(0, a_1, a_2)$. The triangle, square and pentagon labels represent the parameters for panel (a1), (a2) and (a3) in Fig. 2 respectively. (b) Similar as (a) but the chiral term is chosen as $\gamma = \begin{pmatrix} a_1 & a_2 & 0 \\ a_2 & a_1 & 0 \\ 0 & 0 & 0 \end{pmatrix}$. The hexagon corresponds to Fig. 2(a4). (c,d) Phase boundary for chiral terms $\gamma = \begin{pmatrix} a_1 & a_2 & 0 \\ a_2 & a_1 & 0 \\ 0 & 0 & a_3 \end{pmatrix}$ and $\gamma = \begin{pmatrix} a_1 & a_2 & a_3 \\ a_2 & a_1 & 0 \\ a_3 & 0 & a_1 \end{pmatrix}$. The black ball gives the parameters used in Fig. 2(a5).

where the effective ϵ_{eff} along the z direction depends on k_z and ω . Such projection cannot be applied to materials with non-vanishing chiral effects along two directions because there are coupled terms like $\gamma_i \gamma_j, i \neq j$, which lead to the difference in the geometries of EFSs (see Figs. 4(b) and (d)).

Although exceptional points along three spatial directions are decoupled when γ and ϵ (or μ) commute, the situation can be much more complicated if there are non-diagonal terms in the chiral tensor. When there are only diagonal chiral terms, the exceptional points form two intersecting exceptional lines that separate the phase diagram into four parts (Fig. 5(a)). The phase boundary changes when a non-diagonal term is considered (Fig. 5(b)), which is accompanied with some exotic hyperbolic dispersions. In 3D parameter spaces, there exist exceptional surfaces (Fig. 5(c,d)). We see the complex chiral configurations lead to hyperbolic dispersions that cannot be realized in regular HMMs.

Application: all-angle polarization-dependent beam splitter

As we discussed before, a scalar chiral term could render negative refraction but only for a small range of incident angle. This effect is illustrated in Fig. 3(a) as the solid curves, where we choose x - y plane as the plane of incidence, y axis as norm and the incident beam comes from the right side of the norm. The chiral medium locates at $y < 0$ and the region $y \geq 0$ is vacuum. The incident and refraction angles are θ_i and θ_t respectively. The negatively refracted beam disappears when the incident angle exceeds a critical value $\theta_c \sim 36^\circ$, which can be attributed to bounded EFSs. As a comparison, we also plot the θ_i - θ_t relation for a pure dielectric as the dashed curve. There is only one single curve due to the lack of birefringence effect.

Thanks to the hyperbolic dispersion, all-angle negative refraction can be realized in HMMs [15], which is polarization independent. In the \mathcal{CP} -broken region, the hyperbolic dispersion allows the realization of all-angle polarization-sensitive birefringence and negative refraction. We consider a dielectric with chiral vector $\gamma = \text{diag}(0, 2, 0)$, which is in the \mathcal{CP} -broken phase with a type-I hyperbolic dispersion. In Fig. 3(a1), we see that the negative refraction indeed happens for arbitrary incident angles. We further confirm these results through COMSOL simulations, which are plotted in Fig. 3(a2,a3). There is no negative refraction when $\theta_i > \theta_c$ in the \mathcal{CP} -symmetric phase. This effect can be used to engineer an all-angle polarization beam splitter.

Application: enhanced spontaneous emissions for laser engineering

Spontaneous emissions in chiral media have been studied in various situations and exhibit many interesting phenomena. Previous studies have mainly focused on isotropic γ . The \mathcal{CP} breaking through strong anisotropic γ may significantly enhance the spontaneous emissions of a dielectric continuum with both broader bandwidth and stronger Purcell effect due to its hyperbolic bands [17].

Through Fermi's golden rule, we can easily see that the radiative decay rate is generally proportional to the photonic density of states $\rho(\omega) = \sum_{\sigma, \mathbf{k}} \delta(\omega_{\sigma, \mathbf{k}} - \omega)$, where the summation goes over all polarizations σ and momenta \mathbf{k} . The density of state is proportional to the area of EFSs at $\omega_{\sigma, \mathbf{k}} = \omega$, which is a small finite value for dielectrics but diverges for HMMs. Note that it does not diverge in real physical systems due to finite-size effects and corrections of effective medium theory for large \mathbf{k} states [14]. Based on the above arguments, a hyperbolic dispersion would render a larger radiative decay rate and thus, a stronger Purcell effect. The Purcell effect characterizes the enhancement or inhibition of spontaneous emission in a system with respect to free space. For most nanophotonic applications, a stronger Purcell effect (i.e. a larger Purcell factor) is desired.

With the physical understanding, we expect to observe a jump of Purcell factor in chiral medium at a given wavelength k upon crossing the exceptional point and entering the \mathcal{CP} -broken regions. Moreover, the Purcell effect should be much stronger in these cases with exotic hyperbolic dispersions (see Fig. 2(a4,a5)) as they are expected to have larger photonic density of state due to the lack of bounded EFSs.

These expectations are further confirmed by COMSOL simulations as shown in Fig. 3(b). We consider a chiral medium with scale $100\text{nm} \times 100\text{nm} \times 200\text{nm}$ and dielectric constants $\epsilon = 2$ and $\mu = 1$. The chiral terms are $\gamma = (0, 0, \gamma_0)$ and $\gamma = (0, \gamma_0, \gamma_0)$ for each panel. We set $\gamma_0 = 0, 1.4, 1.5, 2$ and 3 for the curves in blue, khaki, green, red and purple colors, respectively. An electric dipole source in vacuum is placed 10nm above the chiral medium in x - y plane and the plotted Purcell factor is averaged through three dipolar configurations along three spatial directions [18]. In the \mathcal{CP} -symmetric regime, the emission strength is essentially unchanged. A substantial enhancement is observed after γ_0 passes the exceptional point and the system enters the \mathcal{CP} -broken regime.

Application: topological photonics

While the current research on topological photonics have focused on periodic systems like photonic crystals, it was recently shown that a continuous HMM is also topologically non-trivial under proper symmetry-breaking fields [25–27]. In this work, we characterize the band structure of chiral medium through the methods developed in [27].

The band structure of a \mathcal{CP} -symmetric chiral medium is plotted in Fig. 2(b) and there cannot be any finite gap no matter how the bands are projected. In this sense, although we may have a strictly quantized Chern number for each bands, this is a trivial phase without any surface state. With increasing γ along z direction, the lower band approaches to the zero plane. Upon passing the \mathcal{CP} breaking point, the upper and lower bands only have one degenerate point in the subspace $k_z \neq 0$ as shown in Fig. 2(b). Such a degeneracy can be easily lifted by anisotropy of ϵ or gyromagnetic effects. After the band gap is opened, the two bands are now topologically non-trivial with a quantized band Chern number and may support chiral surface wave. The only degeneracy in the momentum space is the origin, which is a triply-degenerate point with a topological charge 2 [27].

In Fig. 3(c1), we show the projected 2D band together with the chiral surface wave solutions, where we choose $\epsilon = \text{diag}(3, 2, 1)$, $\mu = I_3$ and $\gamma = \text{diag}(0, 0, 0.5)$. The existence of the chiral surface wave is also confirmed by the COMSOL simulations shown in Fig. 3(c2). The surface wave has different chiralities at $k_z = \pm 1$ due to the non-vanishing charge of triply-degenerate point (breaking \mathcal{P} symmetry). Our results indicate that the non-Hermitian band theory formulated from Maxwell equations for HMMs [27] can also be generalized to chiral dielectric materials.